Available online at www.sciencedirect.com
SCIENCE DIRECT®
Polymer 45 (2004) 825–836
polymer
www.elsevier.com/locate/polymer

Space durable polymer/carbon nanotube films for electrostatic charge mitigation☆

J.G. Smith Jr[a], J.W. Connell[a,*], D.M. Delozier[a,1], P.T. Lillehei[a], K.A. Watson[b,2], Y. Lin[c], B. Zhou[c], Y.-P. Sun[c]

[a]*NASA Langley Research Center, Advanced Materials and Processing Branch, Mail Stop 226, Hampton, VA 23681-2199, USA*
[b]*National Institute of Aerospace, Research Associate, 144 Research Drive, Hampton, VA 23666, USA*
[c]*Howard L. Hunter Chemistry Laboratory, Department of Chemistry, Clemson University, Clemson, SC 29634-0973, USA*

Received 11 September 2003; received in revised form 5 November 2003; accepted 6 November 2003

Abstract

Low color, flexible, space environmentally durable polymeric materials possessing sufficient surface resistivity (10^6–10^{10} Ω/square) for electrostatic charge (ESC) mitigation are of interest for potential applications on Gossamer spacecraft as thin film membranes on antennas, large lightweight space optics, and second surface mirrors. One method of incorporating intrinsic ESC mitigation while maintaining low color, flexibility, and optical clarity is through the utilization of single-walled carbon nanotubes (SWNTs). However, SWNTs are difficult to uniformly disperse in the polymer matrix. The approach reported herein employed amide acid polymers endcapped with alkoxysilane groups that could condense with oxygen containing functionalities that were present on the ends of SWNTs as a result of the oxidative purification treatment. These SWNTs were combined with the endcapped amide acid polymers in solution and subsequently cast as unoriented thin films. Two examples possessed electrical conductivity (measured as surface resistance and surface resistivity) sufficient for ESC mitigation at loading levels of ≤0.08 wt% SWNT as well as good retention of thermo-optical properties. The percolation threshold was determined to lie between 0.03 and 0.04 wt% SWNT loading. Electrical conductivity of the film remained unaffected even after harsh mechanical manipulation.
Published by Elsevier Ltd.

Keywords: Carbon nanotubes; Colorless polyimides; Nanocomposites

1. Introduction

Several proposed space mission concepts envisioned by NASA require the development of large, deployable and ultra-lightweight spacecraft or Gossamer spacecraft [1]. In some concepts, these vehicles partially consist of space environmentally durable polymeric films placed in orbit using conventional launch vehicles. Due to the size of these spacecraft (tens to hundreds of square meters), the films need to be flexible so they can be folded to fit into the available volume of the launch vehicle. Deployment to the final spacecraft configuration would occur on orbit through inflation or mechanical techniques. In addition to being flexible, the film must exhibit a unique combination of physical and mechanical properties depending upon the intended orbit of the vehicle. Physical properties include resistance to many space environmental factors such as atomic oxygen (AO, found predominantly in low Earth orbit), electrons, protons, ultraviolet (UV) and vacuum UV radiation. For some applications, the polymer film must also possess low solar absorptivity (i.e. low color), optical transparency, and high thermal emissivity. Another important physical property needed is sufficient electrical conductivity to mitigate ESC build-up. Exposure of insulating materials such as polymers to a charged orbital environment causes the material to accumulate charge. Since polymeric films are inherently insulative, they can become charged and behave like a capacitor. Discharge can happen in a single

☆ This paper is declared a work of the US Government and is not subject to copyright protection in the United States

* Corresponding author. Tel.: +1-757-864-4264; fax: +1-757-864-8312.
E-mail address: j.w.connell@larc.nasa.gov (J.W. Connell).

[1] National Research Council Research Associate located at NASA Langley Research Center (LaRC), Hampton, VA 23681-2199.

[2] This research was supported in part under NASA Contract No. NAS1-97046 while the author was in residence at ICASE, NASA LaRC, Hampton, VA 23681-2199.

0032-3861/$ - see front matter Published by Elsevier Ltd.
doi:10.1016/j.polymer.2003.11.024

event causing considerable damage to surrounding materials and electronics on the vehicle. To mitigate ESC build-up, a surface resistance in the range of 10^6–10^{10} Ω/square is needed.

Aromatic polyimides are excellent materials for these applications due to their exceptional physical and mechanical properties, as well as radiation resistance. By proper choice of the constituent monomers, low color (i.e. low solar absorptivity) and respectable space environmental durability has been attained [2,3]. However, achieving sufficient electrical conductivity without detriment to other important material properties, particularly transparency and flexibility, has been elusive. One approach to providing sufficient electrical conductivity while maintaining flexibility has involved the addition of single-walled carbon nanotubes (SWNTs) to a polymer matrix [4–7]. It was postulated that the nanotubes would provide sufficient electrical conductivity at a relatively low loading level to mitigate ESC build-up. Due to their low loading level and small size, the effect on the optical properties would be minimal.

Since their discovery, SWNTs were determined to exhibit exceptional mechanical and electrical properties. Improvements in certain mechanical and physical properties of a host polymer compared to the virgin material can be achieved by the incorporation of nanomaterials if the nanomaterials are uniformly dispersed throughout the matrix. This has been difficult to achieve with SWNTs due to the insolubility of the material and/or incompatibility with the host resin. Typically, SWNTs agglomerate as bundles in solvents and the host resin, and if dispersed, reagglomerate soon thereafter due to electrostatic attraction. Good dispersion of SWNTs into LaRC™ CP-2 and other space environmentally durable polymers such as TOR-NC have been reported [4–6]. This was achieved through an in-situ polymerization approach in the presence of SWNTs to form the poly(amide acid)/SWNT mixture with subsequent thermal conversion to the corresponding imide nanocomposite. Alternatively, the amide acid/SWNT mixture can be cyclized chemically in solution provided the imide remains soluble [5,6]. Acceptable conductivity was achieved at ~0.1 vol% loading; however, the films were significantly darker than those from the pristine polymer. A recent approach has involved the coating of SWNTs onto the surface of the polymer film [8]. Whereas the distribution of SWNTs in the bulk provides volume conductivity; the surface coating method affords conductivity on the surface leaving the underlying material and the opposing surface insulative. Due to the low amount (<0.02 wt%) of SWNTs used by this method, the optical transparency and solar absorptivity of the film relative to that of the virgin material were unaffected.

Another means to overcome SWNT insolubility and incompatibility issues has been to functionalize the SWNT through the introduction of carboxylic acid groups [9–12]. Purification of the SWNTs to remove residual catalysts and amorphous carbon has been proposed to introduce functionalities such as carboxylic acid and other oxygen containing species (e.g. hydroxyl groups) at defect sites and tube ends [13–15]. This occurs when the tubes are heated in nitric or nitric/sulfuric acid mixtures.

The approach reported herein involved the use of coupling agent technology to disperse the SWNTs throughout the polymer matrix [6,16]. This technology is based on the use of alkoxysilanes as coupling agents between inorganic substrates (i.e. metals, clays, fibers, etc.) and organic polymers to improve the hot-wet performance of composites and adhesives. The adhesion of the organic surface to the inorganic surface is enhanced through the formation of covalent bonds (i.e. siloxane) between the coupling agent and the inorganic substrate. This bond is formed from condensation of silanol groups on the coupling agent with hydroxyl or carboxyl functionalities present on the inorganic surface. The functionalities present on the inorganic surface may be naturally occurring or generated through chemical reactions on the inorganic surface. In the case of SWNTs, oxygenated functionalities (i.e. hydroxy, carboxyl) are present due to the purification process as previously mentioned.

Alkoxysilane groups have been incorporated into organic compounds and as a polymer substituent through the choice of appropriate monomers or endcapping agents. Amide acid oligomers endcapped with monofunctional alkoxysilanes have been reported [17–23]. Multi-walled carbon nanotubes prepared by a chemical vapor deposition route have been functionalized with butyldimethylsilyl groups by reaction of the appropriate silyl containing compound with polar groups generated on the nanotube surface by acid oxidation [24].

In this work, an alkoxysilane terminated amide acid (ASTAA) polymer of LaRC™ CP-2, a low color space environmentally durable polymer [6,16], was mixed with purified high pressure carbon monoxide (HiPco) prepared SWNTs and thermally cured to afford the corresponding nanocomposite films. By this approach, the SWNTs were added to a pre-made amide acid solution in contrast to the previously mentioned in-situ method. It was postulated that a stable dispersion could be achieved through chemical bond formation with the alkoxysilane endcapped polymer thus lowering the percolation threshold for conductivity, and improving the optical transparency of the nanocomposite. The preparation and characterization of nanocomposite films based on this approach are described herein.

2. Experimental

2.1. Starting materials

The following chemicals were obtained from the indicated sources and used without further purification: aminophenyltrimethoxysilane (APTS, Gelest Inc., ~90% meta, ~10% para), 1,3-bis(3-aminophenoxy)benzene

[APB, Mitsui Chemicals America, Inc. melting point (m.p.) 107–108.5 °C], 3-aminopropyldimethylethoxysilane (Aldrich) and *N*,*N*-dimethylacetamide (DMAc, Aldrich). 4,4′-Hexafluoroisopropylidiene diphthalic anhydride (6-FDA, Hoechst Celanese Inc., m.p. 241–243 °C) was sublimed prior to use. SWNTs prepared by the HiPco process were obtained from Tubes@Rice and purified by heating at 250 °C for ~16 h in a high humidity chamber followed by Soxhlet extraction with hydrochloric acid (22.2 wt%) for ~24 h. All other chemicals were used as-received.

2.2. Model reaction

To a tared vial was added 0.0069 g SWNT and 3 ml of DMAc. The mixture was sonicated at room temperature for ~2.5 h in a Degussa-Ney ULTRAsonik 57X cleaner operated at ~50% power and ~50% degas levels. The initial temperature of the water bath was ambient and ~40 °C at the conclusion of sonication. Then 0.0530 g 3-aminopropyldimethylethoxysilane and 0.1162 g distilled water were added to the mixture. The mixture was shaken on a Mistral Multi-mixer overnight at room temperature. Ethanol was then added to the silylated SWNT/solvent mixture, centrifuged, and the solvent decanted. The silylated SWNTs were dried under vacuum at 50, 75, and 100 °C for 1 h each. The recovery was 0.0114 g silylated SWNTs.

2.3. Alkoxysilane terminated amide acid synthesis

An ASTAA of LaRC™ CP-2 was prepared by the reaction of 6-FDA with APB and end-capped with APTS at a 2.5% offset corresponding to a calculated number average molecular weight ($\overline{M}_n$) of ~27,700 g/mol. First, APB (6.3870 g, 0.0218 mol) and APTS (0.2390 g, 0.0011 mol) were dissolved in DMAc (7 ml) at room temperature under nitrogen. The flask was subsequently immersed in a water bath to dissipate the heat of reaction when the dianhydride was added. Then 6-FDA (9.9547 g, 0.0224 mol) was added in one portion as a slurry in DMAc (10 ml) and rinsed in with 18 ml of DMAc to afford a solution with a solids content of ~33.5%. The reaction mixture was stirred for ~24 h at room temperature under nitrogen. An aliquot was removed to determine inherent viscosity. The remaining solution was used as is or SWNTs were added as described below.

2.4. SWNT–ASTAA mixture

Nanocomposite solutions were prepared by the addition of a sonicated mixture of SWNTs in DMAc to a pre-weighed ASTAA solution. The loadings of SWNTs were 0.03, 0.05, and 0.08 weight (wt)% based on the mass of ASTAA. After stirring at room temperature under a nitrogen atmosphere for ~16 h, the solutions were used to cast unoriented thin films. A representative procedure is described.

To a 100 ml round bottom flask equipped with nitrogen inlet, mechanical stirrer, and drying tube filled with calcium sulfate was charged 11.06 g of an ASTAA solution (~33.5% solids). In a separate tared vial, SWNTs (0.0011 g) were placed in 3 ml of DMAc and the mixture sonicated for ~2.5 h in a Degussa-Ney ULTRAsonik 57X cleaner operated at ~50% power and ~50% degas levels. The initial temperature of the water bath was ambient and ~40 °C at the conclusion of sonication. The suspended tubes were subsequently added to the stirred mixture of ASTAA at room temperature and rinsed in with 4.5 ml of DMAc to afford a solids content of ~20%. The SWNT loading was ~0.03 wt%. The mixture was stirred for ~16 h under a nitrogen atmosphere at room temperature prior to film casting.

2.5. Films

DMAc solutions of the ASTAAs (with and without SWNTs) were doctored onto clean, dry plate glass and dried to tack-free forms in a low humidity chamber at ambient temperature. The films on glass were stage cured in a forced air oven at 100, 200, and 300 °C for 1 h each. The films were subsequently removed from the glass plate and characterized.

2.6. Characterization

Elemental analysis was performed by Desert Analytics (Tucson, Arizona). Inherent viscosity was obtained on a 0.5% (w/v) amide acid solution in DMAc at 25 °C. Differential scanning calorimetry (DSC) was conducted on a Shimadzu DSC-50 thermal analyzer. Melting point ranges (tangent of onset to melt and the endothermic peak) were determined by either DSC at a heating rate of 10 °C/min or visually on a Thomas–Hoover capillary melting point apparatus (uncorrected). Glass transition temperatures (T_gs) were determined by DSC at a heating rate of 20 °C/min and were taken as the inflection point of the ΔH vs. temperature curve. Room temperature thin-film tensile properties were determined according to ASTM D882 using four specimens. Images of the nanocomposites films were obtained at an optical resolution of 200 dpi, medium sharpening, and true color output on a Hewlett Packard HP scanjet 3570c scanner. Ultraviolet/visible/near infrared (UV/vis/NIR) spectra were obtained on thin films using either Perkin–Elmer Lambda 900 or Shimadzu UV3100 UV/vis/NIR spectrometers. Raman spectra were acquired on a Renishaw Raman spectrometer equipped with a 50 mW diode laser source for 780 nm excitation and a CCD detector. High-resolution scanning electron microscopy (HRSEM) images were obtained on Hitachi S-4700 and S-5200 field emission scanning electron microscopy systems operating below 2.0 kV. The composite images were obtained in a low

voltage mode in order to set up a stable local electric field on the sample while minimizing beam-induced damage. Solar absorptivity (α) was measured on thin films using an AZ Technology Model LPSR-300 spectroreflectometer with measurements taken between 250 and 2800 nm. Vapor deposited aluminum on Kapton® film (1st surface mirror) was used as the reflective reference for air mass 0 per ASTM E903. An AZ Technology Temp 2000A infrared reflectometer was used to measure thermal emissivity (ε) of thin films. Surface resistivity was determined according to ASTM D-257-99 using two different devices. The first device utilized an 1863 MΩ meter from General Radio operating at 500 V. Electrodes were painted on the sample with silver paint as parallel lines of a square area. The second device was a Prostat® PSI-870 Surface Resistance and Resistivity Indicator operating at 9 V and reported as an average of three readings. Surface resistance was determined per EOS/ESD Standard S-11.11-1993 using a Prostat® PRS-801 Resistance System operating at 10–100 V and reported as an average of three readings. Volume resistivity was determined using a Prostat® PRS-801 Resistance System with a PRF-911 Concentric Ring Fixture operating at 10–100 V according to ASTM D-257.

3. Results and discussion

3.1. SWNTs

The objective of this work was to develop low color, optically transparent, flexible, space environmentally durable polymers with sufficient conductivity to mitigate ESC build-up. The approach used to incorporate ESC mitigation into the polymer bulk involved the use of SWNTs. The reasons for choosing SWNTs were:

(1) their inherent size, which would potentially have a negligible effect upon the thermo-optical and optical properties of the base polymer,
(2) their high aspect ratio, which suggests that a relatively low loading level would be needed to reach the percolation threshold, and
(3) their high electrical conductivity.

The SWNTs used in this study were prepared by the HiPco process. Due to the preparative method, the SWNTs required purification to remove amorphous carbon and residual catalyst [13,14]. Amorphous carbon was removed by a chemical oxidative process followed by Soxhlet extraction with hydrochloric acid to remove residual iron catalyst. Elemental analysis of the tubes afforded the following results: 89% C, 0.5% H, and 1.8% Fe. As seen from the results, not all of the iron was removed. The residual iron is postulated to be due to residual catalyst inside the nanotube or encased in an amorphous carbon cage. The remaining mass balance (8.7%) is presumably due to oxygen in the form of carbon–oxygen bonded species such as carboxylic acid and hydroxyl groups [13,14] located at defect sites along the tube or at the tube ends. For these SWNTs, the oxygen content was not determined by elemental analysis.

Shown in Fig. 1(A) is a HRSEM image of the purified HiPco SWNTs. Analysis of these SWNTs by atomic force microscopy indicated that the tubes were roped into large bundles ~25 nm in diameter [6]. The images indicated typical SWNTs consistent with other HiPco prepared materials with the following dimensions: ~0.7–1.5 nm in diameter and in the micron range for length. According to the Raman spectrum shown in Fig. 2(A), the radial breathing mode peaks of the purified SWNTs ranged from 170 to 300 cm^{-1}. This suggests a distribution of SWNT diameters in the range of 0.7–1.3 nm [25,26].

To determine the effect of silylation upon the SWNTs, a model reaction was performed using 3-aminopropyldimethylethoxysilane. The mass of the SWNTs increased ~40% after reaction indicating that the alkoxysilane had reacted with the SWNT or adsorbed on the SWNT surface. Since the degree of nanotube functionality is not known, the theoretical yield of product from this reaction cannot be calculated. The formation of chemical bonds between the silanol and functionalities on the nanotubes has been difficult to ascertain by conventional spectroscopic techniques. The HRSEM image of the silylated sample in Fig. 1(B) shows that there is apparently an organic layer covering the SWNTs, which was not present on the purified SWNT starting material in Fig. 1(A). This organic coating was subtle but caused a slight charging effect and gives the CNT a more matted appearance.

The Raman spectrum of the silylated sample (Fig. 2(B)) is similar to that of the starting purified SWNTs (Fig. 2(A)), however some differences in the radial breathing mode are apparent. These differences in the radial breathing mode of the functionalized SWNTs have been observed by others and can be caused by a variety of factors [27–29].

3.2. Nanocomposite synthesis

The polymer matrix used to prepare the SWNT based nanocomposites was a trimethoxysilane endcapped amide acid (ASTAA) of LaRC™ CP-2. The ASTAA polymer was prepared at a stoichiometric offset of 2.5% corresponding to a calculated $\overline{M}_n$ of ~27.700 g/mol (Fig. 3) and had an inherent viscosity of 0.88 dl/g.

The SWNT nanocomposite solutions were prepared by the addition of a suspension of SWNT in DMAc to a stirred solution of an aliquot of the premade ASTAA polymer (Fig. 3). Prior work had shown that films of TOR-NC and LaRC™ CP-2 exhibited conductivities that were acceptable for ESC mitigation at a loading of 0.1 vol% [4,5]. In this work, loadings of 0.03, 0.05, and 0.08 wt% of SWNT relative to the ASTAA polymer were evaluated [6]. The suspended SWNTs were obtained by sonicating the tubes in DMAc.

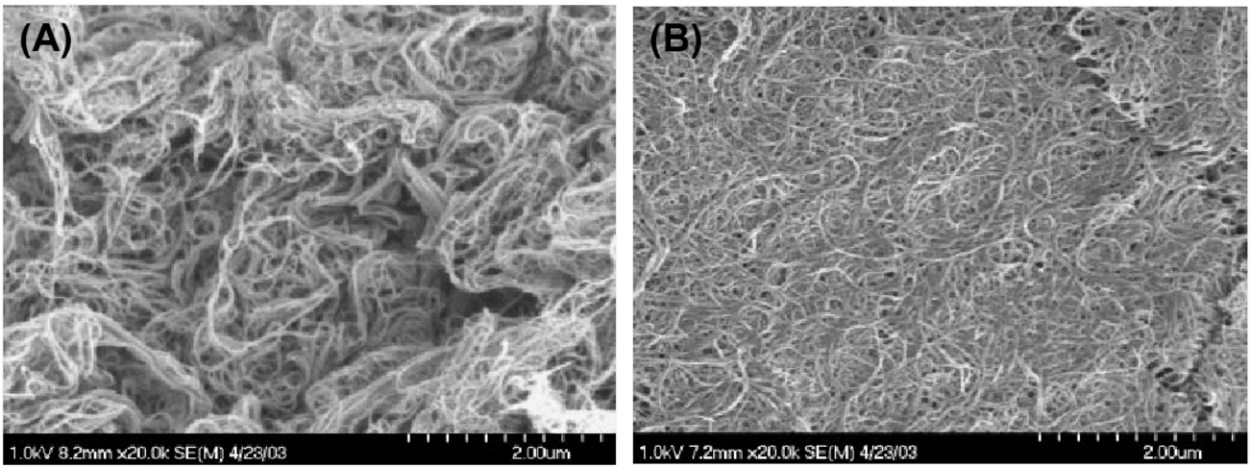

Fig. 1. HRSEM micrographs of HiPco SWNTs (A) before and (B) after silylation.

After the SWNT dispersion was added, the solutions were stirred under low shear with a mechanical stirrer at ambient temperature prior to film casting. The films were dried to a tack-free state and then stage cured to 300 °C in flowing air to effect imidization and condensation. Due to the acidic nature of the amide acid, no additional acid catalyst was required for the hydrolysis of the alkoxysilane endgroups [22]. The silanol groups that are generated can condense with another silanol endcap to form a siloxane chain affording a crosslinked material as shown in Fig. 3. Presumably the silanol can react with carboxylic acid and/or hydroxy functionalities present on the SWNT to form a covalent bond thus aiding in the dispersion (Fig. 4).

3.3. Thermal and tensile properties

The T_g and room temperature tensile properties of the neat polymer (P1) and nanocomposite films (P2–P4) are reported in Table 1. Included are properties for a high molecular weight unendcapped (HMW) version of LaRC™ CP-2 (P5)[3] to compare with the neat polymer endcapped with alkoxysilane groups (P1). A negligible difference in the T_gs of the neat ASTAA based imide (P1) and the HMW, unendcapped material (P5) was observed. This was unexpected since crosslinking tends to increase the T_g of the material with respect to the unendcapped material. However, the tensile properties of P1 were greater than P5 as expected due to the crosslinking provided by the alkoxysilane termination. Most notable was the significant increase in the tensile modulus, which has been previously observed with other alkoxysilane terminated imides [17–23].

The inclusion of SWNTs in the polymer (P2–P4) had a negligible effect upon the T_g and tensile properties compared to P1. These results were surprising since the storage modulus of LaRC™ CP-2 as determined by dynamic mechanical analysis was observed to increase in a linear fashion with increasing SWNT loading [4]. However, a recent report suggests that the dispersed SWNTs may exist as a network structure of aggregated tubes rather than rods and consequently would not provide the anticipated increase in modulus [30]. This network structure was proposed to have a lower modulus as compared to fully dispersed tubes.

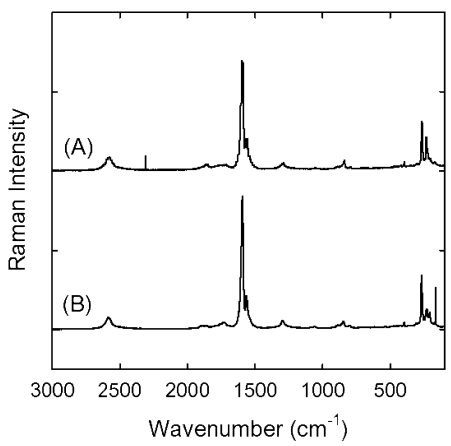

Fig. 2. Raman spectra of HiPco SWNTs (A) before and (B) after silylation.

3.4. Raman and near infrared spectroscopy

The films were examined by Raman spectroscopy to

Table 1
Neat polymer and nanocomposite characterization

ID	SWNT (wt%)	T_g (°C)	Room temperature tensile		Elong @break (%)
			Strength (MPa)	Modulus (GPa)	
P1	0	207	131 ± 4	3.7 ± 0.1	5 ± 1
P2	0.03	205	122 ± 6	3.5 ± 0.2	5 ± 1
P3	0.05	203	139 ± 2	3.7 ± 0.1	6 ± 1
P4	0.08	206	137 ± 6	3.8 ± 0.1	5 ± 1
P5	HMW[a]	209	117	2.9	N.R.[b]

[a] High molecular weight, unendcapped version of LaRC™ CP-2 [3].
[b] N.R.: Not reported.

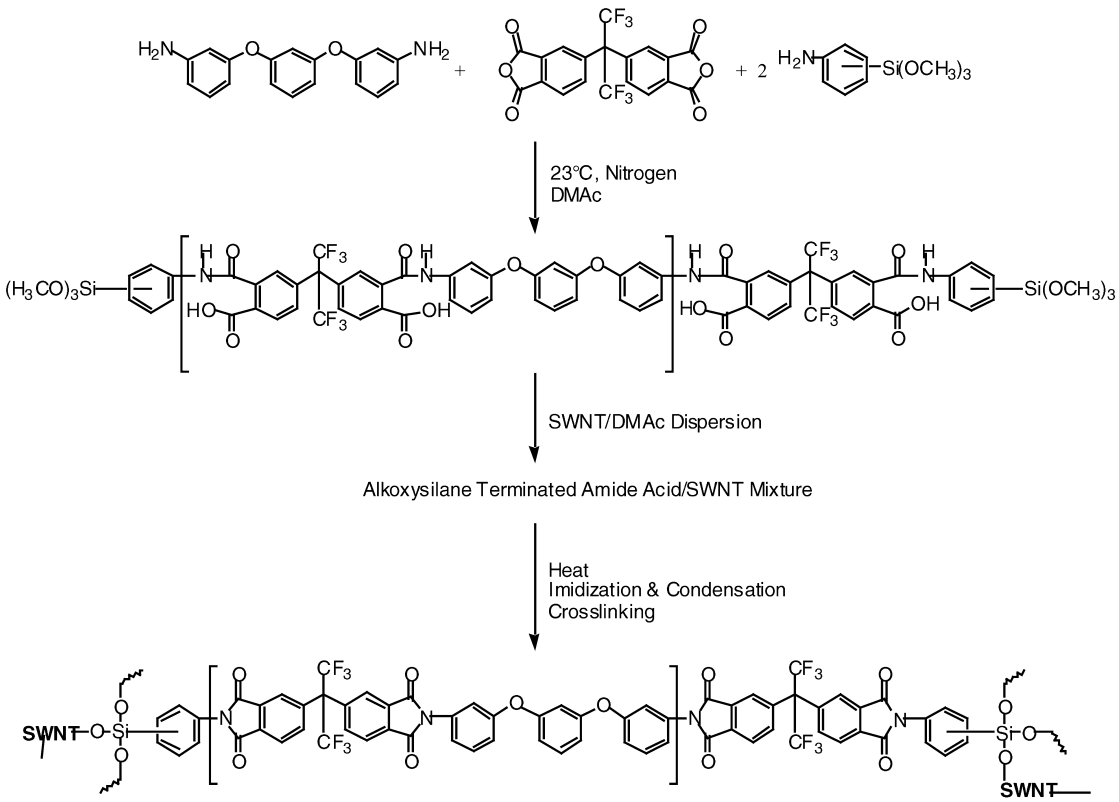

Fig. 3. Synthesis of SWNT nanocomposites from alkoxysilane terminated amide acid polymers.

assess the effect of the chemical reaction between the functionalized SWNTs and the polymer matrix. As shown in Fig. 5, Raman spectra of these nanocomposite films are rather similar exhibiting the typical tangential mode ($\sim$1600 cm^{-1}) and radial breathing mode peaks ($\sim$270 cm^{-1}) over a broad luminescence background. The luminescence is characteristic of chemically modified SWNTs [31,32] and is probably a result of energy trapping by the passivated defect sites on the nanotubes. Additionally, the Raman peaks of the nanocomposite films are fundamentally similar to those of the silylated SWNT sample (Fig. 2(B)) but some minor differences in the radial breathing mode is evident. The stronger Raman intensities observed for P3 compared to P2 and P4 were not meaningful since many factors such as sample thickness, measurement geometry, scattering, etc. may change the intensities. More important are the relative intensities between peaks in the same sample.

The absorption spectra of the nanocomposite films extend well into the near IR region, as shown in Fig. 6. The broad absorption peaks in the 1000–1600 nm ($\sim$0.8–1.2 eV) region are a distribution of transitions associated with the first pairs of van Hove singularities in the density of states of semiconducting HiPco SWNTs of various diameters [25]. Additionally, there are metallic nanotubes in the film samples, as reflected by the small absorption peaks around 600 nm ($\sim$2 eV) [25]. The results suggest that the electronic structures of the SWNTs are largely preserved after modification with organosilane and incorporation into the polymer matrix.

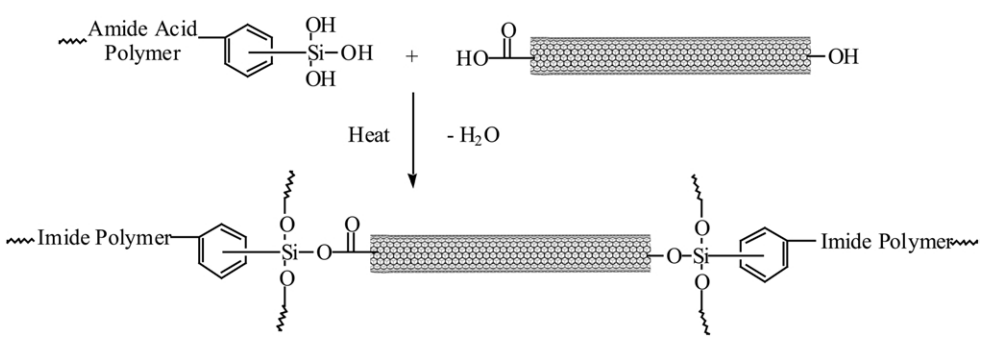

Fig. 4. Postulated reaction between polymer and SWNT.

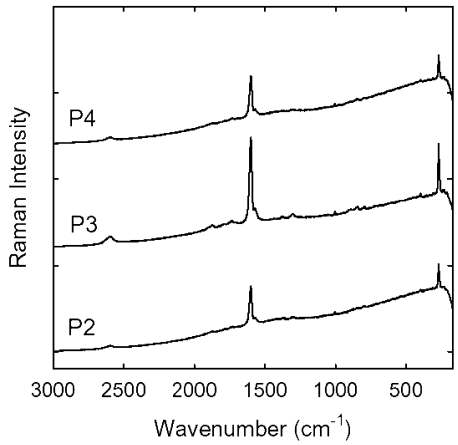

Fig. 5. Raman spectra of nanocomposite films (P2–P4).

3.5. High resolution SEM

To assess SWNT dispersion, P4 containing 0.08 wt% SWNT loading was examined by HRSEM (Fig. 7). Regions of dark contrast in both images are due to the presence of SWNT at or near the surface disturbing the beam-induced electric field [33]. The bright contrast in the cross-section is from the SWNT generating their own secondary electrons. Contrast reversal is seen as the tubes penetrate into the polymer matrix. The cross-section was prepared from a notched tear at room temperature. The two images show that the SWNT are fairly well dispersed throughout the polymer and no large agglomerates are visible, but some localized regions of low and high SWNT concentration are evident. Additionally, regions in the cross-section with no apparent SWNTs are visible. Film P3 containing a 0.05 wt% SWNT loading exhibited a similar appearance. Images of P2 containing a 0.03 wt% SWNT loading could not be obtained due to the nonconductive nature of the sample

3.6. Optical and thermo-optical properties

Of interest was the effect of SWNT inclusion in the polymer matrix upon the % transmission (T) at 500 nm

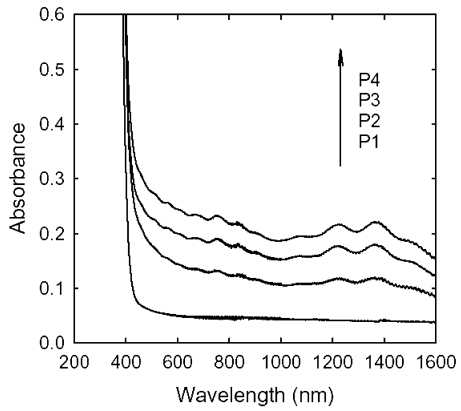

Fig. 6. Absorption spectra of the neat polymer (P1) and nanocomposite films (P2–P4).

(solar maxima), α, and ε; since these properties are important for some Gossamer spacecraft applications. The α pertains to the fraction of incoming solar energy that is absorbed by the film and is low for a low color film ($\sim$0.1 depending upon film thickness). The ε is a measure of the film's ability to radiate energy from its surface. Low α and high ε values are desirable since these films would absorb little radiation and radiate thermal radiation away from the spacecraft. These properties were determined for the HMW unendcapped LaRC™ CP-2 (P5), the neat ASTAA based polymer (P1), and nanocomposite films (P2–P4) and reported in Table 2. Optical properties are known to be thickness dependent and thus all attempts were made to obtain films of comparable thickness. The film thickness ranged from 38 to 41 μm thus allowing comparisons to be made without normalization.

The effect of the endcapping agent upon the optical and thermo-optical properties was determined. It was found that the $\%T$ at 500 nm and α for the neat endcapped (P1) and HMW, unendcapped (P5) materials were comparable. However, ε increased $\sim$10% for P1 as compared to P5. This was presumably due to the alkoxysilane endcapping agent.

Images of the neat polymer (P1) and nanocomposite films (P2–P4) were obtained by directly scanning the films on a flatbed scanner (Fig. 8). As shown, increased SWNT loading resulted in films with increasing darkness. This was also observed by the increase in α from 0.07 to 0.35 and decrease in $\%T$ from 86 to 53.

Since the films were of comparable thickness, $\%T$ was converted to absorbance (A) to determine if the SWNT inclusion adhered to a Beer's Law relationship (Table 2). In a typical Beer's Law experiment, the material of interest is dissolved in a solvent at various concentrations and compared to the neat solvent in a matching cell. However, in this study the solid polymer matrix was the solvent and air was used as the blank. The A of the nanocomposite films (P2–P4) increased with increasing SWNT as compared to P1. Plotting A at 500 nm vs. wt% SWNT loading afforded a Beer's Law relationship (Fig. 9). A linear curve fit of the data had a correlation coefficient of 0.961. At zero concentration in a typical Beer's Law plot the A is zero. The nonzero intercept of the line in the present study is presumably due to scattering and reflection by the film surface(s). The slope of the line is analogous to the extinction coefficient obtained from a Beer's Law plot and was 2.64 $(\text{wt}\%)^{-1}$ for a 38 μm thick film. Dividing the slope by the thickness afforded an extinction coefficient of 0.069 $(\text{wt}\%\ \mu\text{m})^{-1}$ that corresponds to contributions from both the matrix and SWNTs.

The α and ε of the films (P2–P4) likewise increased upon SWNT incorporation relative to P1. Since α is an absorptive property, α vs. wt% SWNT loading was plotted to afford a Beer's Law-like relationship (Fig. 9). This differs from Beer's Law in that α is obtained over the wavelength region of 250–2800 nm. A linear least squares fit of the data

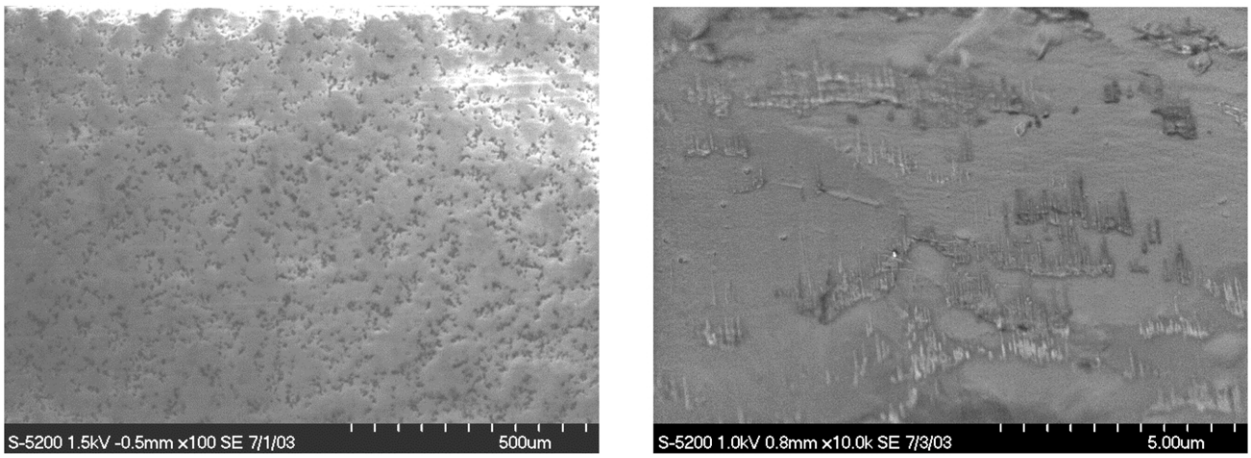

Fig. 7. HRSEM image of nanocomposite film (P4).

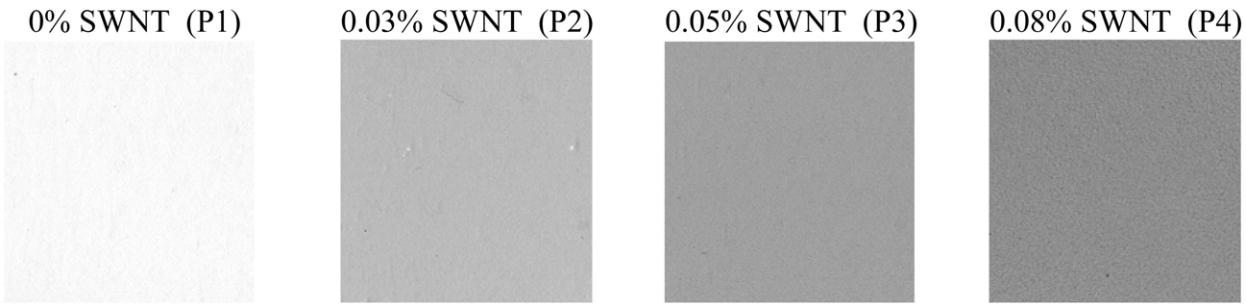

Fig. 8. Neat polymer (P1) and nanocomposite films (P2–P4) obtained by scanning directly on a flatbed scanner.

had a correlation coefficient of 0.951. Note that these relationships (A at 500 nm and α vs. wt% SWNT loading) are presumably dependent on the type, batch, and purity of SWNT used; however, the fundamentals should remain the same.

3.7. Conductivity

Since many of the Gossamer mission concepts require transparent, compliant membranes that will be exposed to the charged orbital environment during their mission, ESC mitigation by intrinsic electrical conductivity while maintaining flexibility in the material is important. Electrical conductivity was determined as surface resistance and surface and volume resistivities (Table 3) and the data plotted vs. wt% SWNT loading (Fig. 10).

Surface resistivity was obtained using two different devices. The first test involved painting silver lines on the sample as parallel lines of a square and subsequently testing the sample with an ohmmeter. By this method, P1 containing no SWNT was insulative as expected. Nanocomposite P2 containing a loading of 0.03 wt% SWNT exhibited a similar result. At a loading of 0.05 wt% SWNT (P3) the percolation threshold had been reached as evident by the sharp drop in the surface resistivity of the material (Fig. 10). Nanocomposites P3 and P4 containing 0.05 and 0.08 wt% SWNT, respectively, exhibited similar surface resistivities. Both values were in a range that was acceptable for ESC mitigation (10^6–10^{10} Ω/square). Similar results were obtained using the Prostat® PSI-870. The order of magnitude differed between the two devices and was likely due to the difference in the voltage that was used to make the

Table 2
Optical and thermo-optical properties of nanocomposites

ID	SWNT (wt%)	Film thickness (μm)	Transmission@500 nm (%)	Absorbance@500 nm	Solar absorptivity, α	Thermal emissivity, ε
P1	0	38	86	0.0655	0.07	0.59
P2	0.03	38	67	0.1739	0.21	0.63
P3	0.05	41	59	0.2291	0.30	0.65
P4	0.08	38	53	0.2757	0.35	0.67
P5	HMW	38	85	0.0706	0.07	0.53

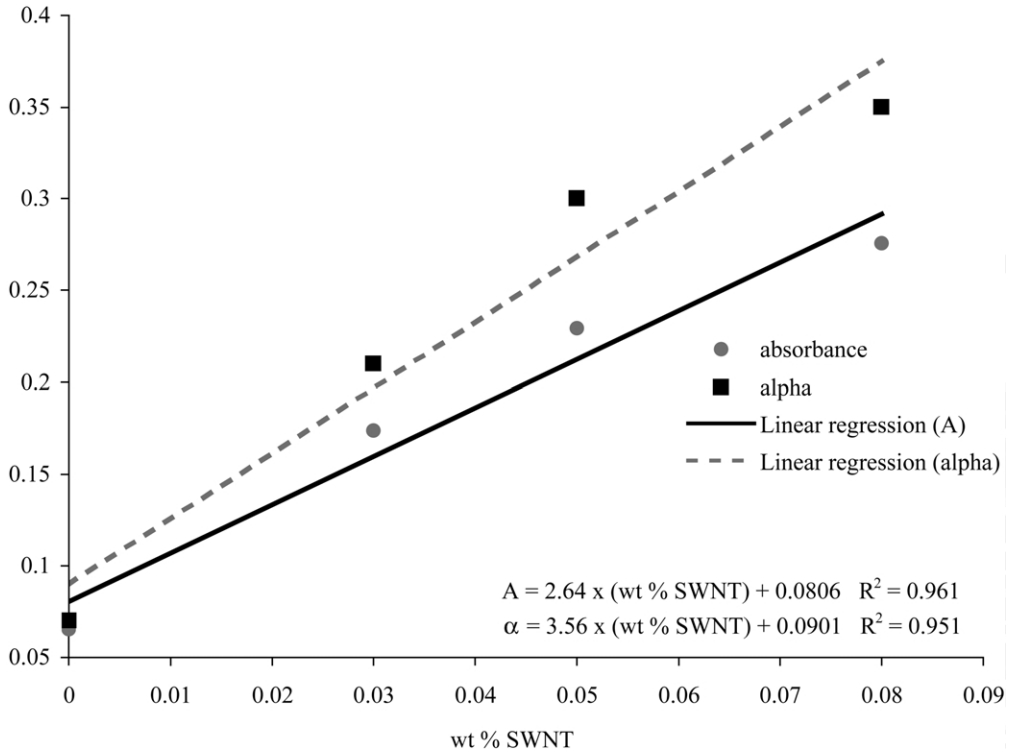

Fig. 9. *A* at 500 nm and α vs. wt% SWNT.

measurements. For the ohmmeter test the voltage was 500, whereas the measurements conducted using the Prostat® PSI-870 was 9.

Surface resistance was determined at 100 V and reported in Ohms. It is the ratio of DC voltage to the current flowing between two electrodes of a specified configuration that contact the same side of the material. Surface resistivity is defined as the electric current flowing across a surface as the ratio of DC voltage drop per unit length to the surface current per unit width and is reported in Ω/square. Surface resistivity is an order of magnitude greater than surface resistance. A more thorough discussion on the relationship between surface resistance and surface resistivity can be found in Ref. [34]. The surface resistance results were comparable to those obtained using the ohmmeter method in that P1 and P2 were insulative while P3 and P4 were conductive.

Volume resistivity was determined on the SWNT containing films (P2–P4). P1 was not measured since it was already shown to be insulative by the other measurements. As seen from the data, a sharp drop in the volume resistivity was achieved at a 0.05 wt% loading. Increasing the wt% loading to 0.08 resulted in a material exhibiting the same order of magnitude resistivity. This data is comparable to that reported above for the surface resistivity and resistance measurements.

Theoretical predictions by analytical modeling have placed the percolation level needed for attaining conductivity as ranging from 0.023 to 0.116 vol% [35]. This corresponds to a single SWNT to a bundle of nineteen tubes at the extremes. In the middle of the range (0.07 vol%), the SWNTs are proposed to exist as a bundle of seven tubes. The results from this study place the percolation threshold at a SWNT loading of 0.05 wt%. However, the tubes are dispersed as bundles and not as individual tubes in the matrix as seen in the HRSEM images (Fig. 7). This is likewise supported by the analytical model that the SWNTs are dispersed throughout the matrix as thin bundles that exist between a single nanotube and a seven-cylinder arrangement [35]. The assumption for the model were for

Table 3
Thin film electrical characterization

ID	SWNT (wt%)	Thickness (μm)	Surface resistivity (Ω/square)		Surface resistance (Ω)	Volume resistivity (Ω cm)
			Ohm meter	Prostat® PSI-870		
P1	0	38	$>10^{12}$	$>10^{12}$	1.4×10^{14}	Not determined
P2	0.03	38	$>10^{11}$	10^{11}	1.5×10^{12}	9.9×10^{14}
P3	0.05	41	1.7×10^{7}	10^{8}	3.9×10^{8}	1.7×10^{9}
P4	0.08	38	9.2×10^{6}	10^{8}	4.5×10^{8}	1.1×10^{9}

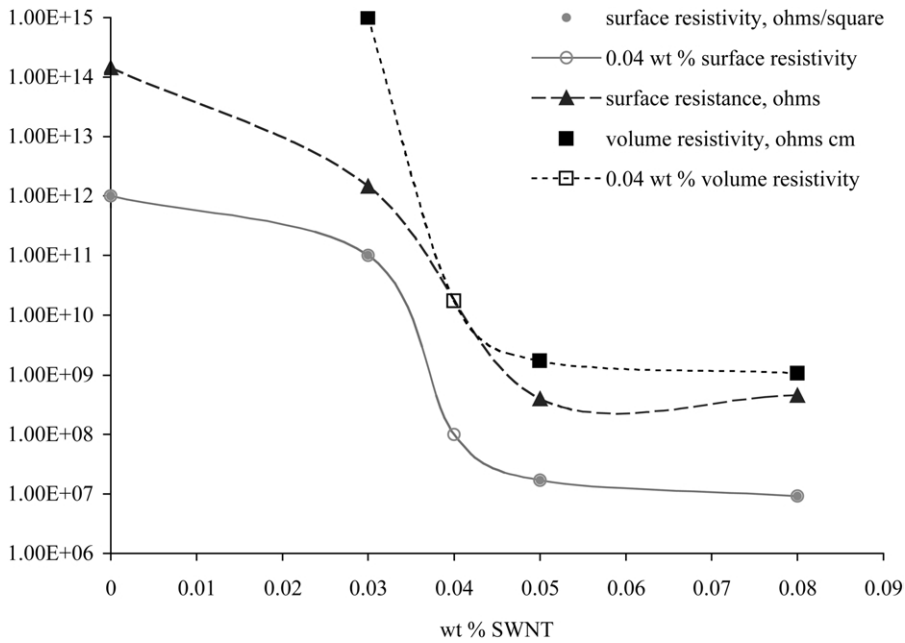

Fig. 10. Surface resistance and surface and volume resistivities vs. wt% SWNT.

unmodified CNTs. The percolation threshold sliding one way or the other may be a reflection of some changes affecting electrical conductivity of the CNTs.

As seen in Fig. 10, the actual wt% loading to achieve the percolation threshold was suggested to lie between 0.03 and 0.05% (w/w) loading using these SWNTs (solid data points). To see if this was the case, a nanocomposite film containing 0.04 wt% SWNT was prepared with the data represented as open markers in Fig. 10. This composition exhibited a surface and volume resistivity of 10^8 Ω/square and 1.7×10^{10} Ω cm, respectively, and suggests that the percolation threshold would lie between 0.03 and 0.04 wt% SWNT loading. These results are consistent with experimental data using untreated catalytically grown SWNTs in an epoxy matrix that suggested the electrical percolation threshold was between 0.0225 and 0.04 wt% [36].

3.8. Flexibility

Besides exhibiting good mechanical and optical properties as well as conductivity to be useful for Gossamer spacecraft, the films need to be flexible. Thus, it was of interest to determine the robustness of the electrical conductivity of these films. Conductive and transparent coatings such as indium tin oxide used on spacecraft are extremely brittle with any folding or bending leading to a loss of conductivity. To assess the robustness of the conductivity of the SWNT nanocomposites, qualitative handling tests were performed on a 38 μm thick film with approximate dimensions of 65 mm by 75 mm containing 0.05 wt% SWNT. The tests involved creasing, folding, and finally crumpling the film into a ball with the surface resistivity measured after every manipulation. The surface resistivity of the unfolded pristine film was 10^8 Ω/square. Fig. 11(A) shows the folded film after seven folds. The film was then unfolded and crumpled into a ball. Fig. 11(B) shows the uncrumpled film after this final manipulation. After all of these mechanical manipulations, the surface resistivity remained unchanged. Additionally, the film retained its integrity and did not fracture or tear. These manipulations were harsh and it is unlikely that the materials on a Gossamer spacecraft would have to endure this degree of abuse during packaging and deployment.

4. Summary

Nanocomposite films were prepared from ASTAAs polymers of LaRC™ CP-2 and HiPco SWNTs. The alkoxysilane termination of the neat polymer was observed to have a negligible effect upon the T_g, optical and electrical properties compared to the high molecular weight version of LaRC™ CP-2; however, the room temperature tensile properties increased. Nanocomposite films containing up to a 0.08 wt% loading of SWNT exhibited similar T_gs and room temperature mechanical properties compared to the neat material. As SWNT concentration increased, the optical and thermo-optical properties decreased. The A at 500 nm and α exhibited a linear dependence upon SWNT wt% loading following a Beer's Law relationship. Sufficient electrical conductivity, as determined by surface and volume resistivity measurements, for ESC mitigation was found for weight loadings of $\geq$0.05%. The percolation threshold to achieve electrical conductivity was determined to be between 0.03 and 0.04 wt% SWNT loading. A 0.05 wt% SWNT containing film exhibited excellent

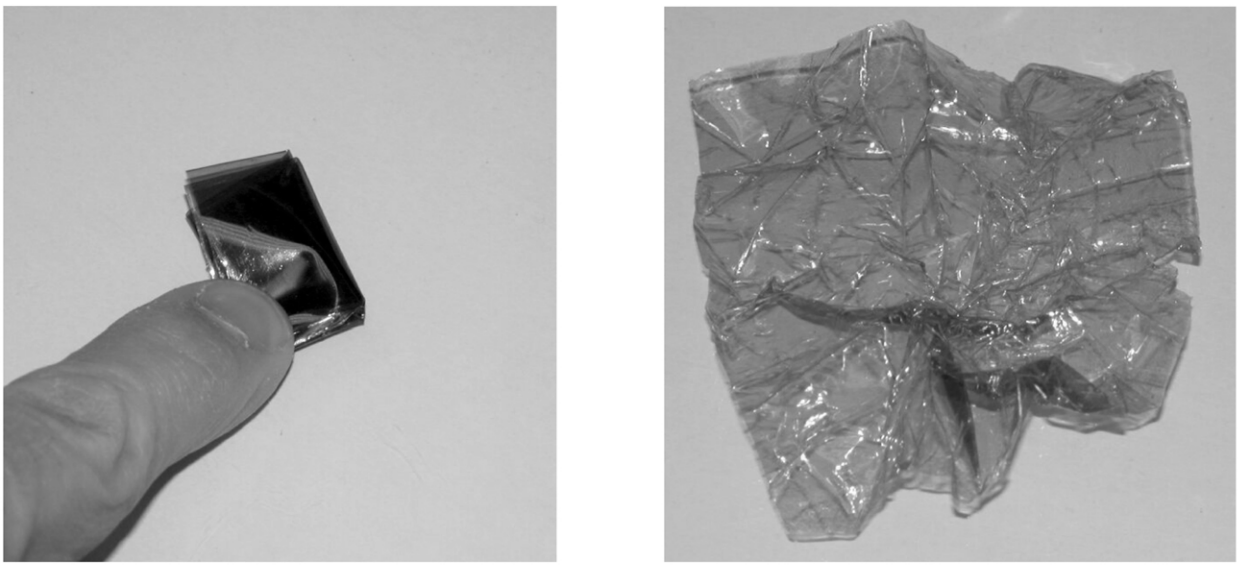

A. Film folded seven times. B. Film after seven folds and crumpled into a ball.

Fig. 11. Mechanical manipulation of a 38 μm 0.05 wt% SWNT film.

flexibility and retention of electrical conductivity after harsh mechanical manipulation. The best combination of properties was obtained for the nanocomposite film with a 0.05 wt% SWNT loading.

Acknowledgements

The authors would like to acknowledge Dr Craig M. Thompson for the thin film tensile testing and Paul Glatkowski of Eikos, Inc., Franklin, MA for determination of the surface resistivity measurements using the Mega Ohm meter. The use of trade names of manufacturers does not constitute an official endorsement of such products or manufacturers, either expressed or implied, by the National Aeronautics and Space Administration.

References

[1] Jenkins CHM, Gossamer spacecraft: membrane and inflatable structures technology for space applications, vol. 191. American Institute of Aeronautics and Astronautics; 2001.
[2] Watson KA, Connell JW, Palmieri FL, Society for the advancement of material and process engineering proceedings, 46; 2001. p. 1853.
[3] SRS Technologies, Huntsville, AL 35806, http://www.srs.com.
[4] Park C, Ounaies Z, Watson KA, Crooks RE, Smith Jr JG, Lowther SE, Connell JW, Siochi EJ, Harrison JS, St. Clair TL. Chem Phys Lett 2002;364:303.
[5] Watson KA, Smith JrJG, Connell JW, Society for the advancement of materials and process engineering technical conference series, 33; 2001. p. 1551.
[6] Smith Jr JG, Watson KA, Thompson CM, Connell JW, Society for the advancement of materials and process engineering technical conference series, 34; 2002. p. 365.
[7] Glatkowski P, Mack P, Conroy JL, Piche JW, Winsor P. US Patent 6, 265,466 B1; July 24, 2001 to Eikos, Inc.
[8] Watson KA, Smith Jr JG, Connell JW, Society for the advancement of material and process engineering proceedings, 48; 2003. p. 1145.
[9] Chen J, Hamon MA, Hu H, Chen Y, Rao AM, Eklund PC, Haddon RC. Science 1998;282:95.
[10] Niyogi S, Hamon MA, Hu H, Zhao B, Bhowmik P, Sen R, Itkis ME, Haddon RC. Acc Chem Res 2002;35:1105.
[11] Sun Y-P, Fu K, Lin Y, Huang W. Acc Chem Res 2002;35:1096.
[12] Hill DE, Lin Y, Rao AM, Allard LF, Sun Y-P. Macromolecules 2002; 35:9466.
[13] Hu H, Bhowmik P, Zhao B, Hamon MA, Itkis ME, Haddon RC. Chem Phys Lett 2001;345:25.
[14] Mawhinney DB, Naumenko V, Kuznetsova A, Yates JT, Liu J, Smalley RE. Chem Phys Lett 2000;324:213.
[15] Bahr JL, Mickelson ET, Bronikowski MJ, Smalley RE, Tour JM. Chem Commun 2001;193.
[16] Smith JG Jr, Connell JW, Lillehei P, Watson KA, Thompson CM. Materials research society spring 2002 symposium T, On-line Proceedings 2002; 733E:T3.5. http://www.mrs.org/publications/epubs/proceedings/spring2002/t/.
[17] Chen Y, Iroh JO. Chem Mater 1999;11:1218.
[18] Fu K, Sun Y-P. J Nanosci Nanotech 2003;3:351.
[19] Beecroft LL, Johnen NA, Ober CK. Polym Adv Tech 1997;8:289.
[20] Srinivasan SA, Hedrick JL, Miller RD, Di Pietro R. Polymer 1997;38: 3129.
[21] Sysel P, Pulec R, Maryska M. J Polym 1997;29:607.
[22] Tsai MH, Whang WT. Polymer 2001;42:4197.
[23] Park C, Lowther SE, Smith Jr JG, Connell JW, Hergenrother PM, St. Clair TL. Int J Adhesion Adhesives 2000;20:457.
[24] Aizawa M, Shaffer MSP. Chem Phys Lett 2003;368:121.
[25] Chiang IW, Brinson BE, Huang AY, Willis PA, Bronikowski M, Margrave JL, Smalley RE, Hauge RHJ. Phys Chem B 2001;105:8297.
[26] Bandow S, Asaka S, Saito Y, Rao AM, Grigorian L, Richter E, Eklund PC. Phys Rev Lett 1998;80:3779.
[27] Bahr JL, Tour JM. Chem Mater 2001;13:3823.
[28] Bahr JL, Yang J, Kosynkin DV, Bronikowski MJ, Smalley RE, Tour JM. J Am Chem Soc 2001;123:6536.
[29] Holzinger M, Abraham J, Whelan P, Graupner R, Ley L, Hennrich F, Kappes M, Hirsch A. J Am Chem Soc 2003;125:8566.

[30] Schafer DW, Zhao J, Brown JM, Anderson DP, Tomlin DW. Chem Phys Lett 2003;375:369.
[31] Riggs JE, Guo Z, Carroll DL, Sun Y-P. J Am Chem Soc 2000;122:5879.
[32] Guldi DM, Holzinger M, Hirsch A, Georgakilas V, Prato M. Chem Commun 2003;1130.
[33] Goldstein J, Newbury D, Joy D, Lyman C, Echlin P, Lifshin E, Sawyer L, Michael J. Scanning electron microscopy and X-ray microanalysis, 3rd ed. New York: Academic/Plenum Publishers; 2003.
[34] Paasi J. Research Note, http://www.vtt.fi/tuo/45/tuloksia/surface_resistance.pdf; March 19, 2002.
[35] Ounaies Z, Park C, Wise KE, Siochi EJ, Harrison JS. Compos Sci Technol 2003;63:1637.
[36] Sandler J, Shaffer MSP, Prasse T, Bauhofer W, Schulte K, Windle AH. Polymer 1999;40:5967.